Electron. Mater. Lett., Vol. 13, No. 1 (2017), pp. 45-50
DOI: 10.1007/s13391-017-6214-6

Effect of O_2 Plasma Treatment on Density-of-States in a-IGZO Thin Film Transistors

Xingwei Ding,[1,2] Fei Huang,[1,3] Sheng Li,[1,2] Jianhua Zhang,[1,2,*] Xueyin Jiang,[3] and Zhilin Zhang[1,3]

[1]Key Laboratory of Advanced Display and System Application, Ministry of Education, Shanghai University, Shanghai 200072, China
[2]School of Mechatronics and Automation, Shanghai University, Shanghai 200072, China
[3]Department of Materials Science, Shanghai University, Shanghai 200072, China

(received date: 3 July 2016 / accepted date: 17 October 2016 / published date: 10 January 2017)

This work reports an efficient route for enhancing the performance of amorphous InGaZnO (a-IGZO) thin film transistors (TFT). The mobility was greatly improved by about 38% by means of O_2 plasma treatment. Temperature-stress was carried out to investigate the stability and extract the parameters related to activation energy (E_a) and density-of-states (DOS). The DOS was calculated on the basis of the experimentally obtained E_a, which can explain the experimental observation. A lower activation energy (E_a, ~0.72 eV) and a smaller DOS were obtained in the O_2 plasma treatment TFT based on the temperature-dependent transfer curves. The results showed that temperature stability and electrical properties enhancements in a-IGZO thin film transistors were attributed to the smaller DOS.

Keywords: thin film transistors, oxygen plasma treatment, density-of-states, a-IGZO

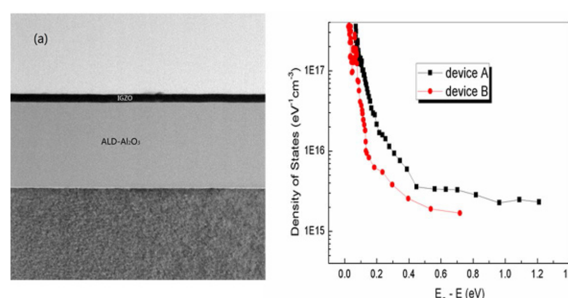

1. INTRODUCTION

a-IGZO, which have been discovered as a TFT material in 2004 by Hosono,[1] have received considerable attention and attracted increasing research interest due to their potential application in the backplane electronics of active matrix organic light emitting diodes (AMOLEDs).[2,3] The carrier concentration in a-IGZO is known to be drastically affected by oxygen-related defects. Especially, the content of oxygen in a-IGZO varies with treatment of the thin film (e.g. with/without O_2 flow during sputtering deposition[4]), so it can greatly affect the electrical properties of the thin film as well as the device performance of the a-IGZO TFTs. In earlier studies, several research groups have studied the effects of O_2 plasma treatment on TFT electrical properties,[4,5] however, many physics of O_2 plasma treatment effects on the density of states still remain unknown. Therefore in this paper, we focused on building a model based on the temperature-stress studies and, thus, revealing how the O_2 plasma treatment affects the DOS and the mechanism of stability.

In this study, we fabricated a-IGZO TFTs under optimized conditions at room temperature, employing Al_2O_3 deposited by atomic layer deposition (ALD) as gate insulator. ALD offers various advantages including accurate thickness and composition control, excellent uniformity and step coverage, low defect density, low deposition temperatures, and good reproducibility.[6-8] Furthermore, as a result of the self-limiting and layer-by-layer (or "digital") growth, ALD exhibits the unique in-situ atomic layer doping capability of achieving precise doping with atomic level control during the deposition process. The fabricated TFT with untreated and O_2-plasma-treated a-IGZO layer was named 'device A'

*Corresponding author: dxw1026@126.com
©KIM and Springer

and ‘device B’, respectively.

2. EXPERIMENTAL PROCEDURE

Bottom-gate TFTs were fabricated on a doped *n*-type Si wafer as shown in Fig. 1. Before being placed in the ALD chamber, the Si substrates were cleaned with consecutive rinses of acetone, isopropyl alcohol, and de-ionized water in an ultrasonicator for 15 min, and then treated by Ozone for 10 min. Immediately following this procedure, Al_2O_3 films of approximately 150-nm-thick were deposited by ALD (TFS-200) technique at 240 °C using $Al(CH_3)_3$ and O_3. The carrier gas was nitrogen of 300 sccm. The purge/pluse time for TMA or O_3 was 7 / 0.1 s. a-IGZO films (99.99%, In: Ga:Zn mole ratio = 1:1:1) were then deposited on to Al_2O_3 film by rf-magnetron sputtering (ULVAC SME-200) at room temperature, a gas mixing ratio of Ar:O_2 (60 : 8) and a power density of 1.8 W/cm^2. A base pressure of 4×10^{-4} Pa, and a working pressure of 0.8 Pa were optimized. We have done the IGZO film treatment by O_2 plasma techniques for 120 s. Al films deposited by thermal evaporation were used for source/drain electrodes through a shadow-mask with the channel width W = 1000 μm and channel length L = 50 μm. Thermal annealing was performed in ambient air at 250 °C for 35 min. The structural property of the films was measured with a high-resolution transmission electron microscopy (HRTEM, FEI Tecnai^{TM} G2 F-20) and X-ray diffraction measurements with Cu-Kα radiation (D/MAX). The electrical properties were performed by using semiconductor parameter analyzer (Agilent, 4155C) with a probe station (LakeShore, TTP4).

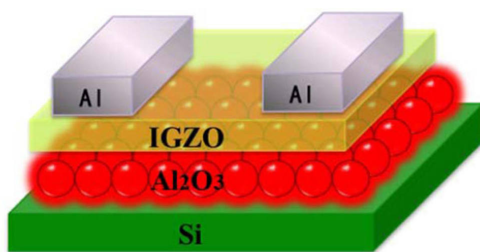

Fig. 1. Schematic structure of the devices.

3. RESULTS AND DISCUSSION

TEM was performed to character the microstructure and thickness of device B as shown in Fig. 2(a). The thickness of a-IGZO is about 15 nm and the value for Al_2O_3 is approximately 150 nm. The interface between a-IGZO and Al_2O_3 is very smooth, which is in favor of the trappings reduction and the carriers transportation.[9] Figure 1(b) shows the XRD pattern of device B. No XRD peak corresponding to Al_2O_3 and a-IGZO is found, which implies that both the insulator and the channel film are amorphous in structure. Almost all metal oxides used for TFT application will form a polycrystalline film during the process of deposition or upon modest thermal treatments, but Al_2O_3 is an exception. Polycrystalline gate dielectrics may cause some problems as the grain boundaries serve as high-leakage paths. In addition, the size of grain and changes of orientation throughout a polycrystalline film may result in significant variations in *k*, which leads to irreproducible properties. In contrary, amorphous film does not suffer from grain boundaries and can easily be manufactured. Therefore, an amorphous Al_2O_3 film structure is ideal for the gate insulator.[10,11]

To examine the effects of O_2 plasma treatment on device performance, the transfer curves of device A and B were measured as shown in Fig. 3. The electrical properties, such as on/off ratio, field effect mobility (μ), threshold voltage (V_{TH}), and sub-threshold swing (*SS*) are summarized in Table 1.

From Table 1 we can see that much better electrical properties are obtained by the O_2 plasma treatment of 120 s. Especially, the filed effect motilities were drastically

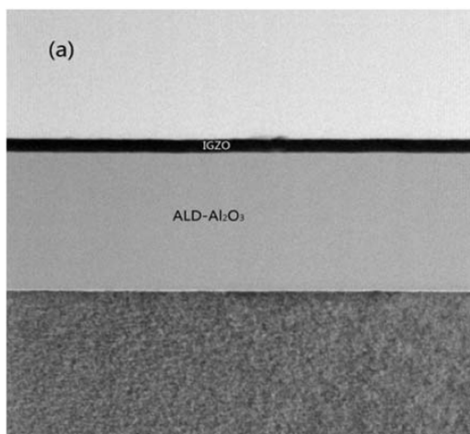

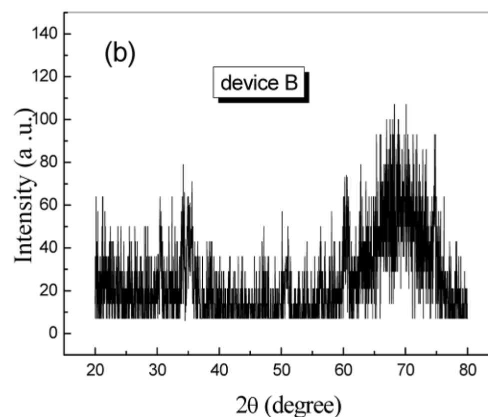

Fig. 2. (a) Cross-sectional TEM images and (b) XRD patten of device B.

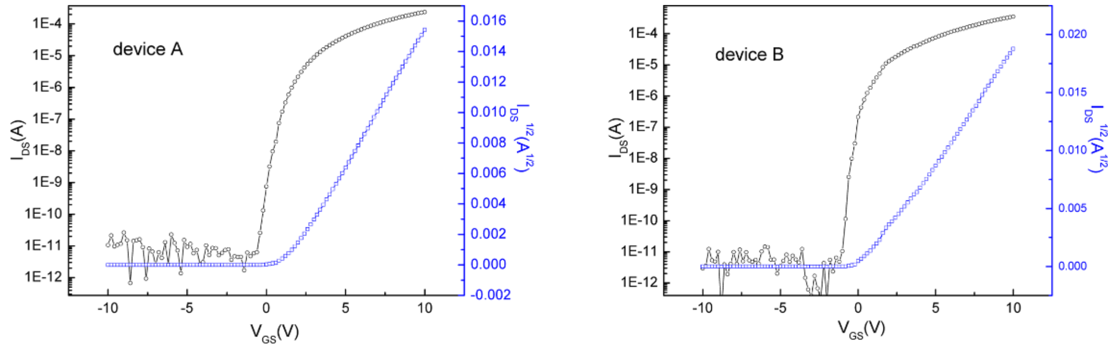

Fig. 3. Transfer curves of (a) device A and (b) device B.

Table 1. Initial electrical characteristics of the devices.

Device	V_{TH} (V)	μ (cm^2/Vs)	on/off	SS (V/dec)
device A	1.35	7.3	> 10^7	0.25
device B	0.49	10.1	> 10^7	0.16

enhanced by about 38%, due to the reduction in oxygen vacancies (a doubly-ionized Vo^{2+} or a singly-ionized Vo^{+}) caused by increased O_2, changes in surface morphology caused by plasma treatment, and differences in trap density at the surface of the channel layer.[12-15]

Temperature stress was carried out to analyze the device stability as shown in Fig. 4. Both devices exhibited a negative shift of V_{TH} as the temperature increased. This phenomenon can be explained by the generation of thermally activated free carriers from deep-level trap sites.[16] The ΔV_{TH} of device B (0.78 V) was smaller than that of device A (2.25 V). At 398 K, stretch-out phenomenon (hump shape) occurred in the sub-threshold regime in undoped a-IGZO TFTs. As shown in Fig. 4(a), the sub-threshold regime was split into normal and stretch-out regions by threshold voltage. This can be explained by Fig. 5(a), i.e. at a gate voltage below V_{TH}, the trap-induced thermal-generated holes move to the source side as a result

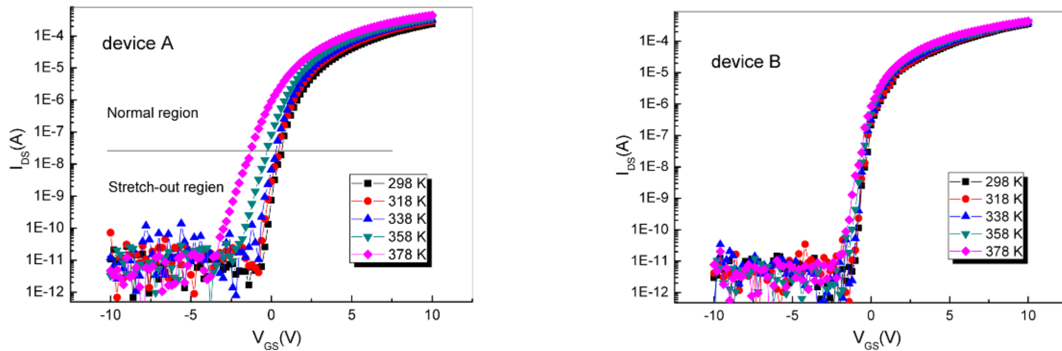

Fig. 4. I_{DS}-V_{GS} curves for device A and B at the different temperatures.

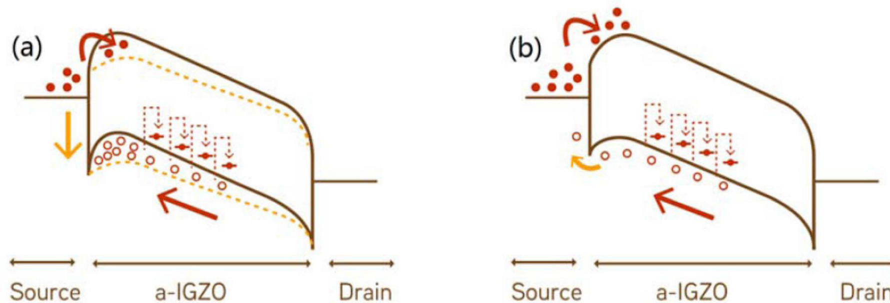

Fig. 5. The energy band diagrams of proposed mechanisms for these two distinctive regions: (a) the gate voltage is below V_{TH} and (b) the gate voltage is above V_{TH}.

of the transverse electric field. Then, the holes accumulated at the source region lead to barrier lowering, which therefore enhances electrons injection from the source and causes an apparent subthreshold leakage current.[17,18] In the normal region, V_{GS} is larger than V_{TH} and the transfer characteristics are dominated by the barrier between the a-IGZO and source. The holes accumulated near the source side flow to the source when the a-IGZO TFTs turn on. As the gate voltage increases, the barrier height becomes much lower, which prohibits the accumulation of holes at the source side, as shown in Fig. 5(b). Therefore, the transfer curve separates into two regions at high temperature.[18,19]

The conductance activation energy (E_a) calculated from the Arrhenius thermal activation model:[20]

$$I_{DS} = I_{D0} \cdot \exp\left[-\frac{E_a(V_{GS})}{kT}\right] \tag{1}$$

where E_a is the activation energy, I_{DS} is the drain current in subthreshold region, I_{D0} is the prefactor, k is the Boltzmann constant, and T is the temperature. The relation between E_a and V_{GS} is shown in Fig. 6. In the sub-threshold current region, the decrease of E_a occurs with increasing gate voltage, which should have the same magnitude as the upward shift of E_F to E_C.[18,21] The maximum of E_a (1.21 eV) for device A is larger than that (0.72 eV) of device B, which is attributed to the O_2 plasma treatment.[22,23] It was reported that the change rate of E_F with respect to V_{GS} ($\Delta E_F/\Delta V_{GS}$) is in inverse proportion to the magnitude of N_{total} when a TFT has a significantly large trap density (N_{total}) including the DOS of a semiconductor film (N_{SS}) and an interfacial trap density (N_{it}). As all the trap sites below E_F must be filled with electrons before they can move to the E_F level in the forbidden bandgap region.[2,24] The falling rate (~ 0.9 eV/V) of E_a in device B is much faster than that (~ 0.64 eV/V) in device A, suggesting that a N_{total} value of device B is reduced compared to device A. Therefore, device B exhibits a faster moving E_F level with respective V_{GS}, which indicates the reduction in bulk and interface trap density.[25]

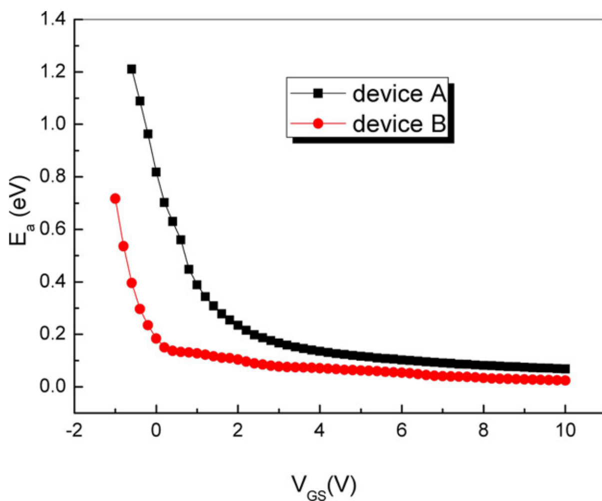

Fig. 6. Extracted active energy (E_a) as a function of V_{GS}.

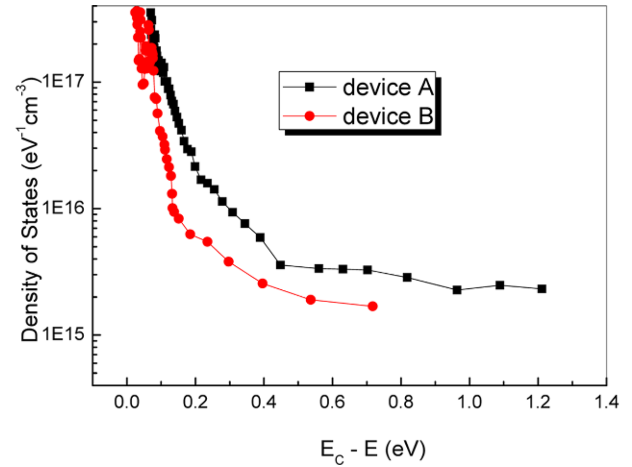

Fig. 7. Calculated DOS distribution as a function of the energy (E_C-E) for devices.

The method of calculating DOS are described in our previous work[26] based on the following equation:[27]

$$g(E_a) = -\frac{\varepsilon_i}{q d_i t \dfrac{dE_a}{dV_{GS}}} \tag{2}$$

Figure 7 shows the DOS distribution for devices. A much smaller total DOS for device B compared to that of device A over the entire tailing energy range extracted further suggests superior performance of device B, implying that O_2 plasma treatment has a positive effect on the improvement of TFT performance. The total DOS value at a specific energy level is the summation of N_{it} and N_{SS} because both trap states hinder the moving up of the E_F level at the interface with increasing V_{GS} ($>V_{FB}$).[28] Based on DOS results, we conclude that the device A has much more bulk traps and interface trap states than those of the device B. Therefore, the improved performances in device B can be caused by the reduction in total traps causes. Using O_2 plasma treatment is an effective way to improve the electrical performance and stability of a-IGZO TFT.

We carried out XPS measurement on devices to further confirm the effect of O_2 plasma treatment on the electrical properties. Figure 8(a) and (b) show the XPS spectra of O1s for device A and B, respectively. According to Gaussian fitting, peaks of O1s are combined and consistently fitted into three different peaks including a low binding energy (O_L), a medium binding energy (O_M), and a higher binding energy (O_H). The O_L component is ascribed to the O^{2-} ions surrounded by Ga, In and Zn ions. The O_M peak can be attributed to the deficiently bonded oxygen in the IGZO material with the non-stoichiometric oxide species such as

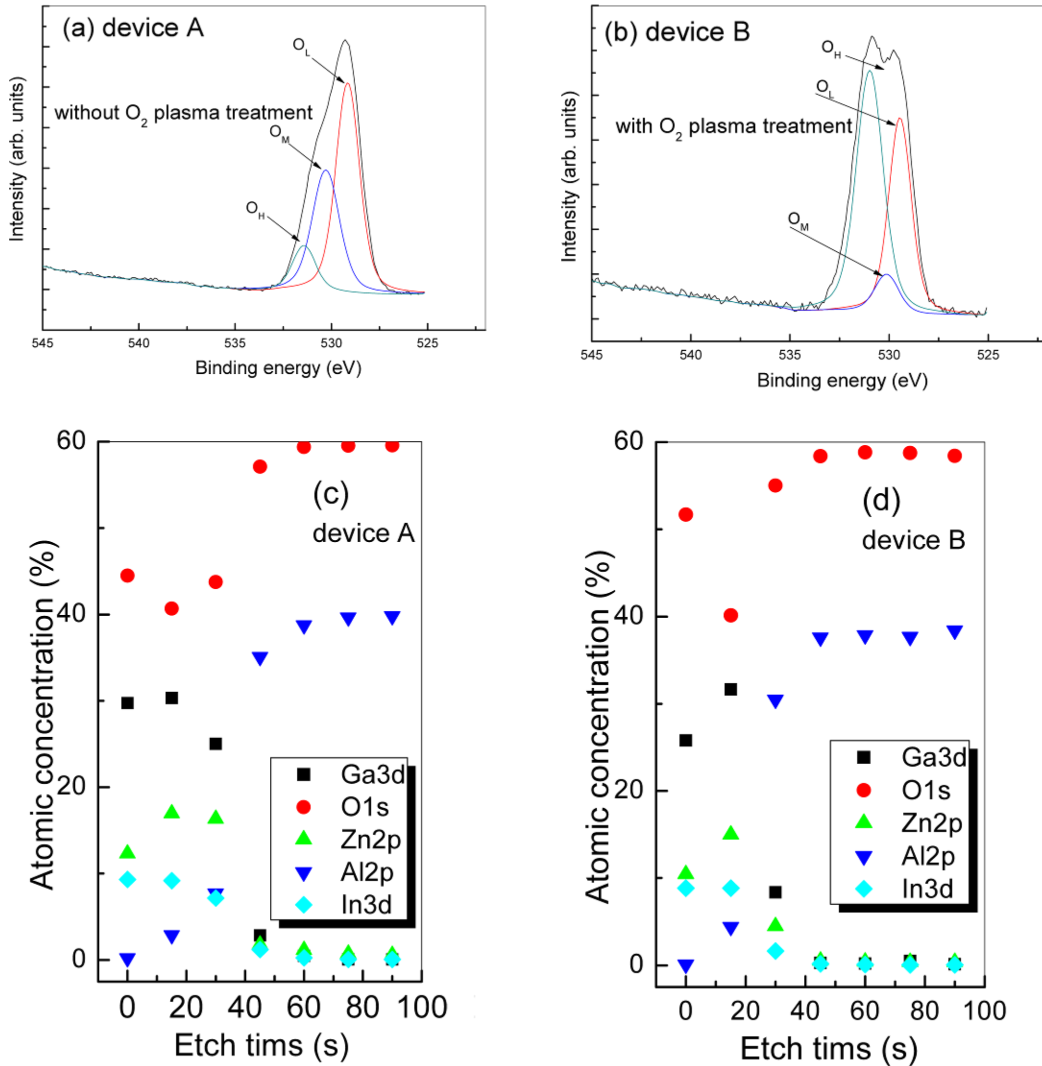

Fig. 8. XPS spectra of O1s for (a) device A (without O_2 plasma treatment); (b) device B (with O_2 plasma treatment); Concentration-depth profile of (c) device A and (d) device B.

In_2O_{3-x}, ZnO_{1-x}, Ga_2O_{3-x}.[4,29] The chemisorbed oxygen on the film surface and the grain boundaries of the a-IGZO film contributes to the O_H peak.[30] It can be seen from the figure that both O_L and O_M decrease after the O_2 plasma treatment while O_H increases. Before the immersion, the ratio of O_L/ O_M is 1.5 and it increases to 4.3 after the immersion, which indicates that deficiently bonded oxygen in the IGZO matrix decreases after the O_2 plasma treatment. As a result, the electron concentration decreases along with the decrease in the density of the oxygen-related defects because they act as donors in the n-like IGZO semiconductor. The results suggest that the density of states for a-IGZO with O_2 plasma treatment is much lower than that without plasma treatment. Fig. 8(c) and (d) shows the atomic concentration for device A and B with different etch times, respectively. Both the devices have the same atomic concentration at the interface, implying that the O_2 plasma treatment is hard to invade the interface.

4. CONCLUSIONS

In this paper, the O_2 plasma treatment for a-IGZO TFT was studied. The transfer curve exhibits an apparent subthreshold current stretch-out phenomenon at 378 K which becomes serious with increasing temperatures. After O_2-plasma treatment, the devices exhibit superior electrical properties. Significantly improved electrical properties and temperature stress stability are obtained in the O_2 plasma treatment TFT due to the reduced DOS, to be specific, a high field effect mobility of 10.1 cm^2/Vs, a suitable threshold voltage of 0.49 V, a high on/off ratio of over 10^7, a steep sub-threshold swing of 0.16 V/dec, and a substantially small

threshold voltage shift of 0.78 V after temperature stress from 298 K to 378 K.

ACKNOWLEDGEMENT

This work is supported by the Project of National Post-Doctor Fund (2015M580315) and the National Natural Science Foundation of China (61077013, 61274082, 51072111, and 51302165).

REFERENCES

1. K. Nomura, H. Ohta, A. Takagi, T. Kamiya, and H. Hosono, *Nature* **432**, 488 (2004).
2. K. H. Ji, J. I. Kim, H. Y. Jung, S. Y. Park, Y. G. Mo, J. H. Jeong, J. Y. Kwon, M. K. Ryu, S. Y. Lee, R. Choi, and J. K. Jeong, *J. Electrochem. Soc.* **157**, H983 (2010).
3. T. Oh, *Electron. Mater. Lett.* **11**, 853 (2015).
4. P. Liu, T. P. Chen, Z. Liu, C. S. Tan, and K. C. Leong, *Thin Solid Films* **545**, 533 (2013).
5. W.-S. Kim, Y.-K. Moon, S. Lee, B.-W. Kang, K.-T. Kim, J.-H. Lee, J.-H. Kim, B.-D. Ahn, and J.-W. Park, *Jpn. J. Appl. Phys.* **49**, 08JF02 (2010).
6. R. L. Puurunen, *J. Appl. Phys.* **97**, 121301 (2005).
7. L.-L. Zheng, Q. Ma, Y.-H. Wang, W.-J. Liu, S.-J. Ding, and D. W. Zhang, *IEEE Electr. Dev. L.* **37**, 743 (2016).
8. H.-Y. Shih, F.-C. Chu, A. Das, C.-Y. Lee, M.-J. Chen, and R.-M. Lin, *Nanoscale Res. Lett.* **11**, 1 (2016).
9. X. Ding, H. Zhang, J. Zhang, J. Li, W. Shi, X. Jiang, and Z. Zhang, *Mat. Sci. Semicon. Proc.* **29**, 69 (2015).
10. G. D. Wilk, R. M. Wallace, and J. M. Anthony, *J. Appl. Phys.* **89**, 5243 (2001).
11. X. Ding, H. Zhang, H. Ding, J. Zhang, C. Huang, W. Shi, J. Li, X. Jiang, and Z. Zhang, *Superlattice. Microst.* **76**, 156 (2014).
12. H. Faber, J. Hirschmann, M. Klaumünzer, B. Braunschweig, W. Peukert, and M. Halik, *ACS Appl. Mater. Interfaces* **4**, 1693 (2012).
13. S. W. Ko, S. K. Kim, J. M. Kim, J. H. Cho, H. S. Park, and B. D. Choi, *J. Nanosci. and Nanotechno.* **15**, 7476 (2015).
14. C. J. Chiu, Z. W. Pei, S. T. Chang, S. P. Chang, and S. J. Chang, *Vacuum* **86**, 246 (2011).
15. K. Nayak, M. N. Hedhili, D. K. Cha, and H. N. Alshareef, *Appl. Phys. Lett.* **100**, 202106 (2012).
16. H. C. Slade, M. S. Shur, S. C. Deane, and M. Hack, *Appl. Phys. Lett.* **69**, 2560 (1996).
17. G.-W. Chang, T.-C. Chang, J.-C. Jhu, T.-M. Tsai, Y.-E. Syu, K.-C. Chang, Y.-H. Tai, F.-Y. Jian, and Y.-C. Hung, *IEEE Electr. Dev. L.* **33**, 540 (2012).
18. J. Raja, K. Jang, N. Balaji, and J. Yi, *Semicond. Sci. Technol.* **28**, 115010 (2013).
19. A. Indluru and T. L. Alford, *IEEE T. Elec. Dev.* **57**, 3006 (2010).
20. K. Takechi, M. Nakata, T. Eguchi, H. Yamaguchi, and S. Kaneko, *Jpn. J. Appl. Phys.* **48**, 011301 (2009).
21. B. D. Ahn, Y. S. Rim, H. J. Kim, J. H. Lim, K.-B. Chung, and J.-S. Park, *J. Phys. D: Appl. Phys.* **47**, 105104 (2014).
22. J. K. Jeong, S. Yang, D.-H. Cho, S.-H. K. Park, C.-S. Hwang, and K. I. Cho, *Appl. Phys. Lett.* **95**, 123505 (2009).
23. H. Wang, W. Xu, S. Zhou, F. Xie, Y. Xiao, L. Ye, J. Chen, and J. Xu, *J. Appl. Phys.* **117**, 035703 (2015).
24. D. H. Kim, H. K. Jung, D. H. Kim, and S. Y. Lee, *Appl. Phys. Lett.* **99**, 162101 (2011).
25. S. Y. Lee, D. H. Kim, E. Chong, Y. W. Jeon, and D. H. Kim, *Appl. Phys. Lett.* **98**, 122105 (2011).
26. J. Zhang, X. Ding, J. Li, H. Zhang, X. Jiang, and Z. Zhang, *Ceram. Int.* **42**, 8115 (2016).
27. Y. H. Tai, H. L. Chiu, and L. S. Chou, *J. Electrochem. Soc.* **159**, J200 (2012).
28. G.-W. Chang, T.-C. Chang, J.-C. Jhu, T.-M. Tsai, Y.-E. Syu, K.-C. Chang, F.-Y. Jian, Y.-C. Hung, and Y.-H. Tai, *Surf. Coat. Tech.* **231**, 281 (2013).
29. S. Jeong, Y. G. Ha, J. Moon, A. Facchetti, and T. J. Marks, *Adv. Mater.* **22**, 1346 (2010).
30. S. Major, S. Kumar, M. Bhatnagar, and K. L. Chopra, *Appl. Phys. Lett.* **49**, 394 (1986).